Observational Study

Medicine®

OPEN

Effects of the attenuation correction and reconstruction method parameters on conventional cardiac dynamic SPECT

Mohammadreza Mohseni, MSc[a,b], Reza Faghihi, PhD[b,c], Mahdi Haghighatafshar, MD[a,*], Seyed Mohammad Entezarmahdi, MSc[a,d]

Abstract

Nuclear cardiology has not witnessed development of new tracers or hardware for many years. Hence there is a need for the development of improvised techniques. Dynamic cardiac single photon emission computed tomography (SPECT) is one such technique that has a potential to overcome the limitations of conventional myocardial SPECT including the absolute quantification of blood flow. The main goal of this study is to evaluate the effect of attenuation correction (AC) on estimation of the washout parameters extracted from dynamic SPECT using a conventional protocol. The effect of the postprocessing on quantitative evaluation of dynamic SPECT is also assessed.

A physical phantom was employed to physically simulate the dynamic behavior of a heart in the thorax. Using a dual detector SPECT system, 180° tomographic data in every 90 seconds were acquired. The SPECT data were reconstructed using ordered subset expectation maximization (OSEM) method while different iterations and a Butterworth filter with different cut-off frequencies were applied. Estimated washout parameter of the time activity curves (TACs) was compared with applying AC or without it.

Results show that AC can improve the bias of computed washout parameter in normal regions (average bias reduction in normal ROI: 7%). Moreover, the postreconstruction filtering and reducing the number of iterations in reconstructing phase can reduce the variance of the computed washout values in normal regions (from 3.99% for cut-off frequency 0.5 cycle/cm and 32 times update in OSEM to 2.05% for cut-off frequency 0.35 cycle/cm and 16 times update in OSEM). They also reduce the actual size of the defect region (13% reduction in defect extent for above change in reconstruction parameters).

According to the results, the AC and postprocessing filtration can directly affect the standard deviation of washout value acquired by cardiac dynamic SPECT. These parameters also showed a direct effect on the defect extent in final results. The study showed that the AC may partly improve the bias of calculated normal washout value. The effect of attenuation correction on the defective washout value could not be answered comprehensively in this paper.

Abbreviations: AC = attenuation correction, CAD = coronary artery diseases, DSPECT = dynamic single photon emission computed tomography, FOV = field of view, FWHM = full width at half maximum, LV = left ventricle, MBF = myocardial blood flow, MLEM = maximum likelihood expectation maximization, OSEM = ordered subset expectation maximization, PET = positron emission tomography, ROI = region of interest, SPECT = single photon emission computed tomography, TAC = time activity curves.

Keywords: attenuation correction, dynamic SPECT, phantom, reconstruction

1. Introduction

Single photon emission computed tomography (SPECT) imaging is one of the most important clinical techniques in nuclear medicine[1,2] especially for diagnosis of coronary artery diseases (CAD).[3,4] Dynamic cardiac SPECT imaging method is one of the proposed methods in nuclear cardiology which has the potential to extract both kinetic and perfusion information for evaluation of CAD, and may provide more accurate measurement of myocardial stiffness development in comparison with static im ages.[5,6] However, quantification of myocardial blood flow (MBF) at stress and rest and determination of the myocardial dynamic parameters have been the domain of PET myocardial perfusion imaging (MPI) with tracers such as $^{13}NH_3$-ammonia, ^{15}O-water, and ^{82}rubidium. While dynamic parameters such as blood flow measurements with PET obtain easily, myocardial perfusion SPECT is currently is the major examination for MPI analysis. SPECT MPI is also a significantly cheaper modality. While the SPECT systems are widely available, if it were indeed feasible to estimate the dynamic parameters from the standard SPECT MPI scan, it would dramatically enhance the clinical usage of this examination.[7] Also no new radiotracers and hardware have been suggested for many years, so new methods such as dynamic cardiac SPECT may offer the only potential to improve risk stratification in cases of CAD. Dynamic imaging could be performed on every cardiac SPECT procedure to provide improved lesion contrast and better evaluation of viable myocardium. However, there are challenges in the improvement

Editor: Gaurav Malhotra.

This was the MSc thesis of Mohammadreza Mohseni and was supported by Nuclear Medicine and Molecular Imaging Research Center, Shiraz University of Medical Sciences, Shiraz, Iran (reference No. 8153).

The authors have no conflicts of interest to disclose.

[a] Nuclear Medicine and Molecular Imaging Research Center, Namazi Teaching Hospital, Shiraz University of Medical Sciences, [b] Nuclear Engineering Department, [c] Radiation Research Center, Shiraz University, Shiraz, [d] Radiation Medicine Engineering Department, Shahid Beheshti University, GC, Tehran, Iran.

[*] Correspondence: Mahdi Haghighatafshar, Nuclear Medicine and Molecular Imaging Research Center, Namazi Teaching Hospital, Shiraz University of Medical Sciences, Shiraz, Iran (e-mail: afsharm@sums.ac.ir).

Copyright © 2018 the Author(s). Published by Wolters Kluwer Health, Inc. This is an open access article distributed under the terms of the Creative Commons Attribution-Non Commercial-No Derivatives License 4.0 (CCBY-NC-ND), where it is permissible to download and share the work provided it is properly cited. The work cannot be changed in any way or used commercially without permission from the journal.

Medicine (2018) 97:39(e12239)

Received: 26 June 2017 / Accepted: 11 August 2018

http://dx.doi.org/10.1097/MD.0000000000012239

of hardware, radiopharmaceuticals, and data processing techniques for dynamic cardiac SPECT to understand all its potential.[8] Compared with conventional static imaging, dynamic SPECT (DSPECT) data acquisition and quantitative kinetic data analysis provide unique information that can enable improved discrimination between healthy and unhealthy tissue[9] and also some information on myocardium flow abnormalities are provided.[10] A central assumption in SPECT is that the projection data are "constant," that is, the camera views a stable radiotracer distribution during acquisition while using 99mTc-Sestamibi (MIBI) as radiotracer.[11] But when wash-in and washout rate of blood into cardiac muscle is desired to be measured, detector is faced with change in radiotracer distribution in the region of interest (ROI) both inter- and intraprojections. That is why conventional SPECT imaging is not able to reveal quantitative information about the biophysiological or bio-mechanical processes.[12] On the other hand, the rotation speed of conventional SPECT cameras is relatively less than what is needed to record the activity distribution changes so yield temporally inconsistent projection data.[13] Therefore modified acquisition protocols are used.[14]

In order to acquire the DSPECT, the various SPECT systems, acquisition protocols, reconstruction algorithms, and postprocessing methods have been reported.[9,15–17] There are at least 2 methods suggested for estimating kinetic data using DSPECT; the extraction of dynamic information directly from projections and the conventional approach by constructing a sequence of three-dimensional (3D) images, drawing ROIs, generating TAC for these regions, and then estimating kinetic model parameters from these TACs.[18] For generating TAC in this study the second method has been employed and just the washout quantity is measured.

As in positron emission tomography (PET), correction for attenuation in SPECT seems to be vital. Based on the previous studies, it is probable that AC is effective to establish absolute myocardial blood flow (MFB) measurement in cardiac SPECT.[19] In Hutton and Ben-Haim[20] paper it seems that the AC is a vital correction among other corrections, while some others clearly show that specially when a rational parameter such as myocardial blood flow is extracted from the dynamic SPECT the AC has no significant effect. Since DSPECT imaging suffers from low signal-to-noise ratio, due to short scan time, it is still needed to evaluate the effect of attenuation correction on DSPECT imaging.[21] Also, iterations and subsets in OSEM reconstruction method and cut-off frequency of Butterworth post-filter are of interest but have controversies.[22–25]

Based on the foregoing, the purpose of this study is to evaluate the effect of AC and some of reconstruction and postprocessing parameters on DSPECT results. Some enhanced physical phantoms were used in this study so that the experiment comes close to the real-imaging situation. A conventional acquisition protocol was employed and based on the prior known TACs[26] the amount of activity of each segment (normal myocardium, defective myocardium, blood pool and trunk) was modified for every single projection.

2. Materials and methods

This study has been approved by the Ethics Committee and Institutional Review Board of Shiraz University of medical sciences (Study Code No. 1393-01-01-8153).

2.1. Compartmental modeling

A compartment is a volume or space in which the tracer is uniformly distributed; which means there is no considerable concentration gradient within the volume.[27] A compartment can be a physical space such as an organ, or a metabolic or bound state of the tracer.[18] A one-compartmental model, which is also used in this study, is shown in Figure 1. In this model, blood activity assumed to be constant and known so the blood is not considered as a compartment. Differential equation representing the activity changes between the extravascular and blood is as follows:[18]

$$\frac{dC_{EV}(t)}{dt} = K_1 \cdot B(t) - k_2 \cdot C_{EV}(t) \quad (1)$$

where K_1 and k_2 are cardiac kinetic parameters. $B(t)$ is the blood activity at time t and C_{EV} is the extravascular activity concentration at time t. In this equation, the rate of changes in/out of extravascular space is proportional to the blood/extravascular activity concentration.

The activity concentration in a ROI would be

$$A(t) = F_V \times B(t) + (1 - F_V) \times C_{EV}(t) \quad (2)$$

where $A(t)$ can be activity at time t in a region of myocardium, F_V is vascular fraction of blood in the tissue, and $(1-F_V)$ is the fractional extravascular volume.

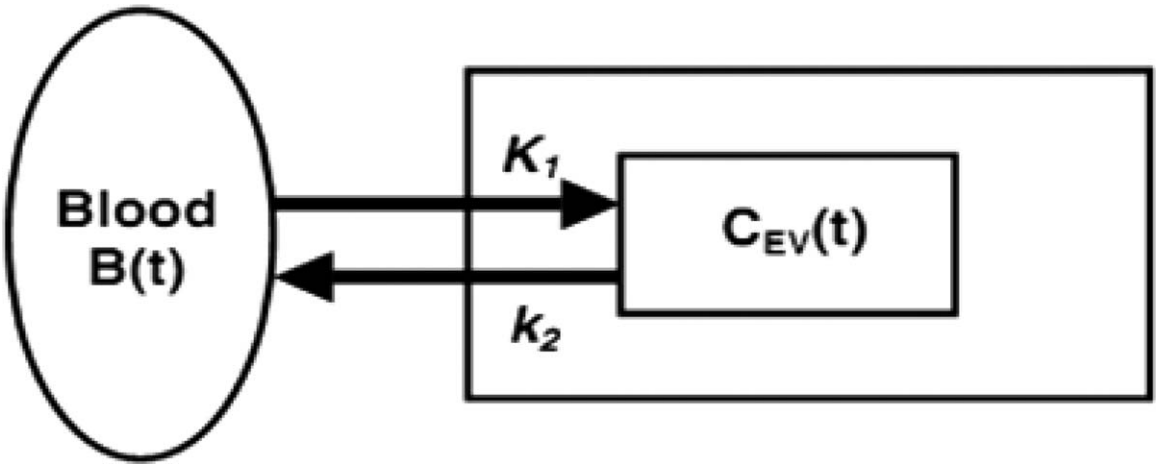

Figure 1. One-compartment model. Extravascular region is the only existing compartment in the model.

Solution to Eq. (1) is

$$C_{EV}(t) = K_1 \cdot \int_0^t B(\tau) \cdot e^{-k_2(t-\tau)} d\tau = K_1 \cdot e^{-k_2 t} \otimes B(t) \quad (3)$$

where means convolution. By substituting Eq. (3) in Eq. (2) and assuming that the blood activity is known, the result will be

$$A(t) = F_V \times B(t) + (1 - F_V) \times K_1 \times e^{-k_2 t} \otimes B(t) \quad (4)$$

If just the washout rate coefficient of TAC (variation of radiotracer within myocardium after 160 seconds postinjection) is desired, B can be considered constant and independent of time.

With this assumption the simple form of the above equation after 160 seconds will be

$$= C_1 + C_2 \times e^{-k_2 t} \quad (5)$$

In Eq. (5), the coefficient k_2 indicates the radiotracer washout rate of the tissue. The coefficient C_1 shows the amount of activity remaining in the tissue. Aggregation of C_1 and C_2 shows the amount of activity deposited in the tissue at 160 seconds postinjection.[28] In this paper, we will estimate the priori known k_2 to evaluate the effect of AC and postprocessing methods.

2.2. Phantom preparation

A standard cardiac phantom (cardiac insert, manufactured by Biodex medical systems) was used in order to simulate blood pool and myocardium. A fillable defect phantom which is a peripheral to the cardiac insert phantom set was used to simulate the myocardial defect.

Cardiac insert was put into a Jaszczak phantom (Flanged Deluxe Phantom Model ECT/DLX/P) full of water, along with background activity of body, for simulating trunk which is origin of noise and scatter. In this study no bone presence (ribs) was considered. The most important reason of using physical phantom is simulating real data acquisition situation. Noises related to data acquisition system and environmental noise exist in physical simulation which cannot be thoroughly taken into account when using digital phantoms, despite the fact that random noise can be applied in digital phantoms. Also, there is no center or rotation error (caused by finite accuracy of acquisition system) in computer simulation while it may happen when using physical phantoms. Typical TACs for different segments of heart are known and used in other studies.[10,26] TACs for different organs are drawn in Figure 2. From Figure 2, some relative activity amounts in different time points were extracted. Then, an exponential equation, such as mentioned in Eq. (5), was fitted to these sample points from the moment when the blood pool TAC is constant (after 160 second postinjection) using Levenberg–Marquardt method. After that, according to these estimated

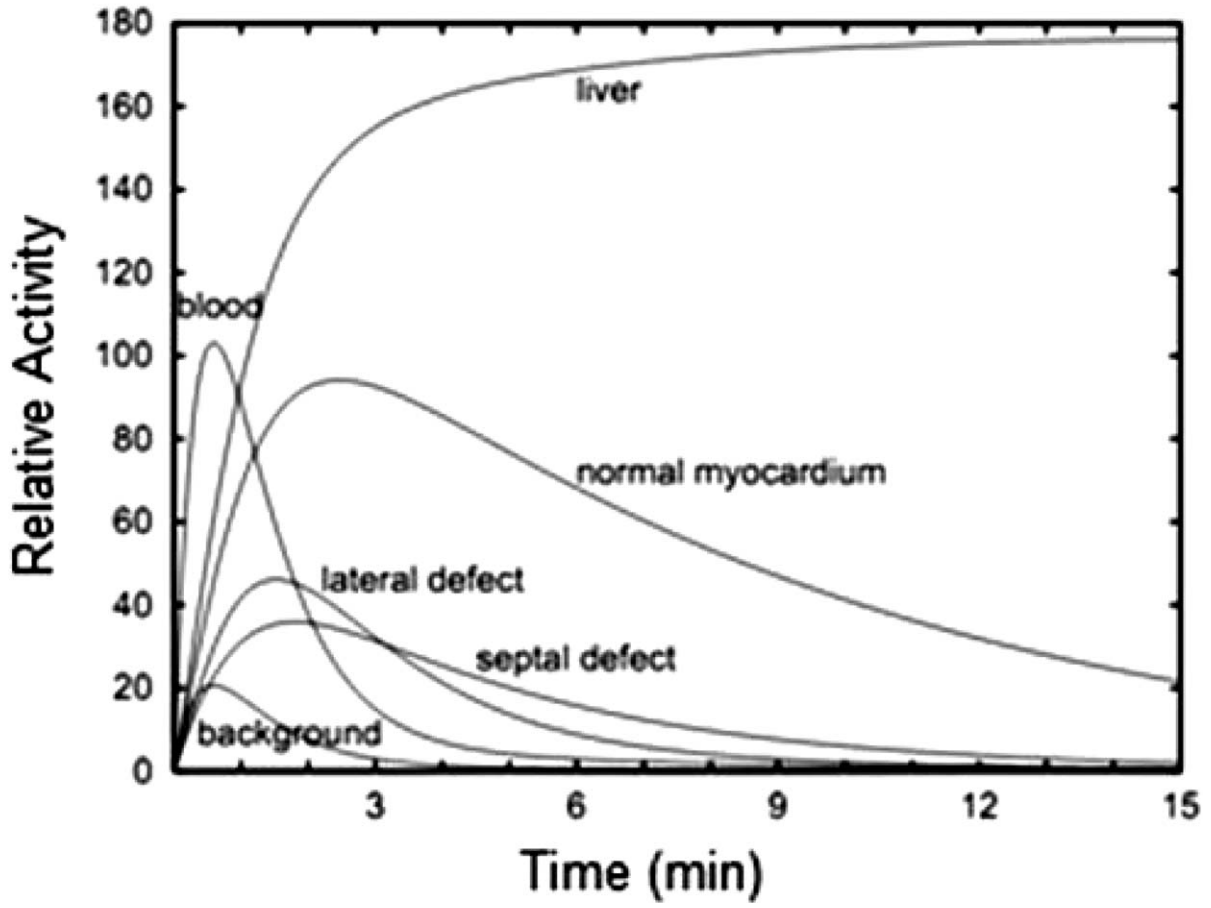

Figure 2. TAC for liver, blood, background, normal myocardium, and defective myocardium.[22] TAC = time activity curves.

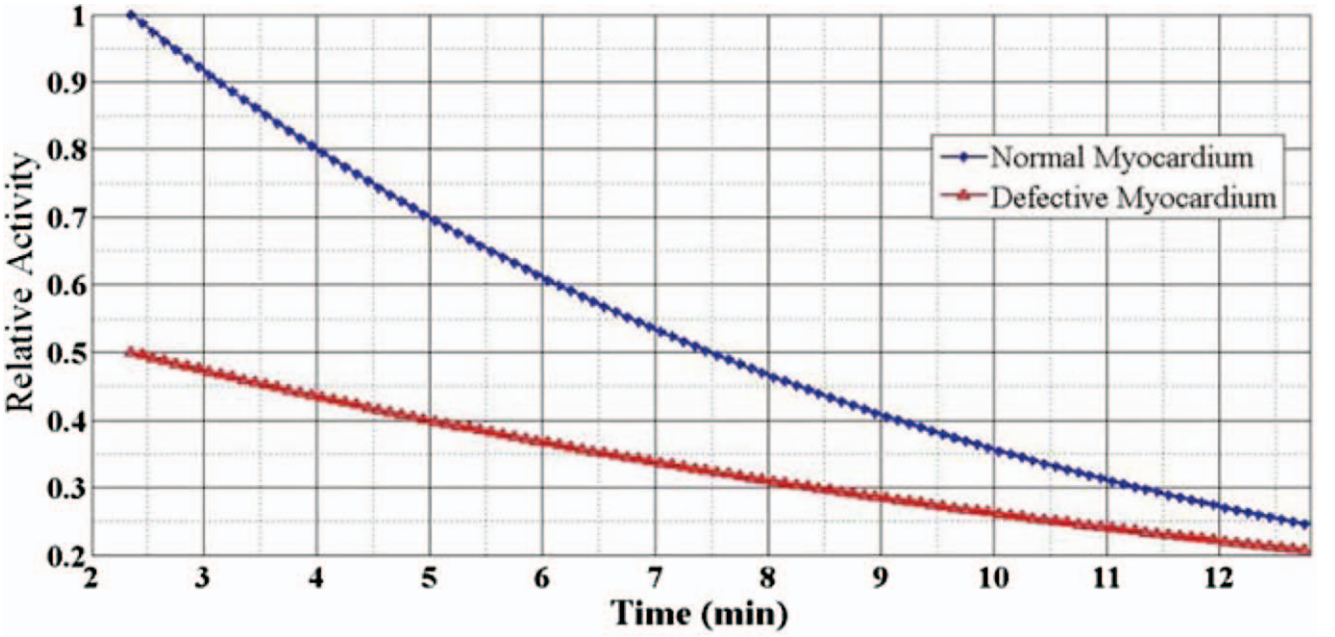

Figure 3. Re-drawn TACs for normal and defective myocardium. TAC = time activity curves.

equations [Eqs. (6) and (7)], normal and defective myocardial TACs were drawn as in Figure 3.

$$\text{Relative activity for normal region} = a \times e^{-0.135 \times t} \quad (6)$$

$$\text{Relative activity for defective region} = b \times e^{-0.084 \times t} \quad (7)$$

For every single projection taken by gamma camera, activities within the myocardium and blood pool were modified and calibrated based on Eqs. (6) and (7) (Fig. 3). Injected activity into myocardial phantom was 200 MBq at the highest level. To access the defective part of myocardium from the outside of the phantom and simulate its dynamic behavior some physical modification was applied to the cardiac insert and its defect phantom which is shown in Figure 4. The defect content was accessible with a hose from outside of the tank. This hose is placed in the mid-part of inferoseptal wall. In the hose coupling point, the radioactivity concentration was somehow out of control. Therefore the mid-inferoseptal portion of the left ventricle (LV) wall shows higher washout rate in all reconstructed images. To verify that reported high washout rate originated from the hose coupling, the experiment was repeated with different defects (with variation both in size and position). All the experiments show the same phenomenon in the hose coupling point. In Figure 5, the approximate position of defect is obtained.

Comparing applied TAC to the phantom and extracted curve from the reconstructed images, effects of AC application and different postprocessing in DSPECT can be evaluated.

2.3. Data acquisition

A dual-head gamma camera (Hawkeye4 Infinia, GE Medical Systems, Inc., Waukesha) was used in this study that was equipped with low-energy, high-resolution collimators; the heads were at 90° to each other (onto a 64×64 matrix). In order to carry out data acquisition, a DSPECT protocol was provided based on the protocols used previously.[16] Acquisition protocol consisted of 5 alternative clockwise and counterclockwise 180° rotations. In each rotation, a total of 15 projections were sampled over 90° for each detector. Each view was acquired for 5 seconds. SPECT images were obtained in step-and-shoot mode and moving time from one view to the next view was 2 seconds. Also, after each 180° rotation, switching time from one direction (clockwise) to the other direction (counterclockwise) took 29 seconds. Aggregation time for this protocol (from very beginning to the end of the last view) was 640 seconds. The phantom set simulates a patient lain in a head-first supine position. Following the emission tomography, a transmission tomography was performed to obtain an attenuation map as follows: 140 kVp, 2.5 mA, 5 mm slice thickness, axial acquisition with 5.0 mm interval, full per slice, velocity 2.6 RPM. Reconstruction parameters were as follows: matrix 512×512, filter standard and extended FOV).

2.4. Image reconstruction

To reconstruct the emission images in this study, ordered subsets expectation maximization (OSEM) was utilized. OSEM is an accelerated version of maximum likelihood expectation maximization (MLEM). OSEM method is almost the same as MLEM except that the each iteration in OSEM includes several subiterations. Reconstruction time for OSEM is less than what is needed in MLEM but the quality of the reconstructed image with OSEM is the same as the image produced with MLEM.[17]

2.5. Image processing:

Overall, 5 set of projection series are acquired. Each of them was reconstructed into a single image using OSEM reconstruction method while different reconstruction parameters were used. The result was 5 images from phantom for each set of parameters. Number of iterations, maximum number of subsets, and different cut-off frequencies (for Butterworth post-filter) were the parameters which vary in different reconstruction methods.

Figure 4. Modified cardiac inset.

Each of these methods was performed with and without AC. Reconstructed images were segmented and analyzed with Corridor-4DM software package (INVIA, Ann Arbor, University of Michigan Medical Center). The next step was estimation of washout rate coefficient from the reconstructed images. Polar map of each reconstructed image was partitioned based on 17 segments model.[29]

Counted events for each pixel of selected regions in the polar map were recorded. The same trend is followed for other images. The recorded values were normalized to the first rotation maximum count and time ordered. Then an exponential curve was fitted over the values with the Levenberg–Marquardt method; so the washout rate was estimated for all of the pixels. The color of each pixel in the final polar maps indicates the normalized tracer washout rate coefficient for that individual pixel. In order to investigate the effects of AC and different reconstruction methods on TAC in normal and defective regions of the cardiac phantom, the extracted washout rate with and without the AC and with different reconstruction methods was calculated.

2.6. Statistical analysis

IMB SPSS was employed to evaluate the effectiveness of AC and the effects of reconstruction parameters. The paired samples *t*-test was performed (with confidence interval of 95%) on washout rates obtained from attenuation corrected and non-corrected pixels with different reconstruction methods. All statistical tests were 2-tailed and a P value $< .05$ was considered to indicate statistical significance. Such evaluation was performed on every method used in this study. Since this study was phantom based ethical approval was waived.

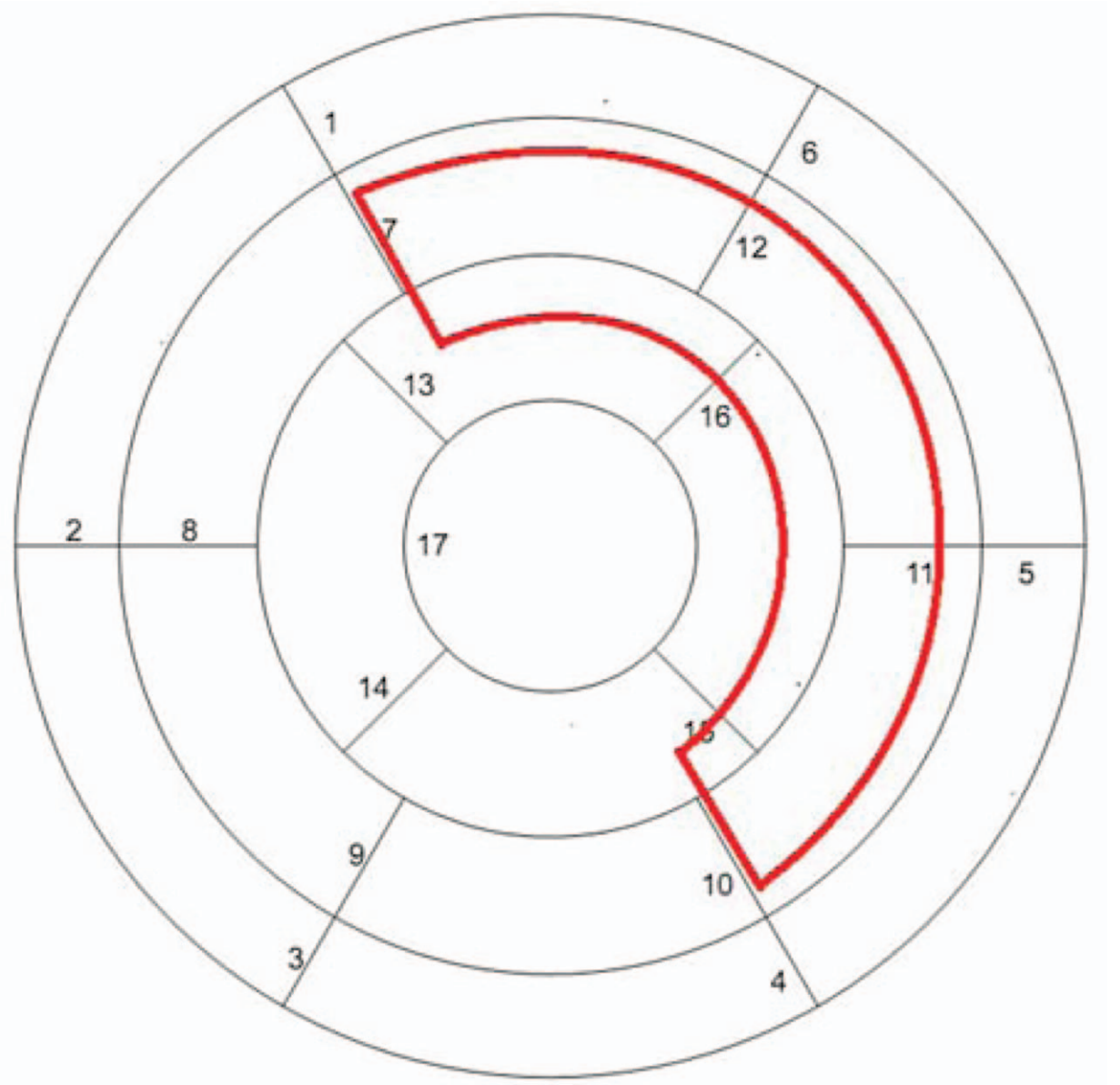

Figure 5. The approximate position of defect in a polar map view.

3. Results

Figure 6A shows the polar maps for nonattenuation corrected images while OSEM reconstruction method with different iterations and subsets was followed by a Butterworth post-filter while different cut-off frequencies (cycle/cm) and power of 10 were applied. Figure 6B and C shows the results with and without attenuation correction while different cut-off frequencies and different iterations were applied. As mentioned before, color intensity of the reconstructed images in Figure 6A–C indicates the estimated normalized washout rate coefficient for each pixel. Wash-out rate coefficient interval of these figures is typically in the scale of 0.025 to 0.155.

To quantify differences in defect extent, disk-like profiles through the center of the defects within polar maps were calculated. The profiles extracted from polar maps in Figure 6A–C are presented in Figure 7. Full width at half maximum (FWHM) of these figures represents the extent of defect in different reconstructed methods. Table 1 shows the FWHM of these profiles for different reconstruction methods.

So, to evaluate the effects of different postprocessing methods on the calculated washout rate, an ROI was plotted manually in the defect region by an expert physician. This ROI was mirrored into the inferoseptal segment to evaluate normal rate variations. Table 2 shows the results of the ROIs analysis.

Mean value of estimated washout rates to the desired rate, 0.135, which is the desired washout rate of normal part in the experiment, in percentage for each segment was displayed in Figure 8A and B. These data were extracted when OSEM reconstruction algorithm with 3 iterations and 8 subsets (OSEM 3, 8) followed by a Butterworth post-filter with 0.5 cycle/cm and power of 10 (BW, 0.5, 10) were applied. Absolute mean value of estimated washout rate for each segment is obtained in parenthesis below the percentage rates. Figure 8A presents the values when no attenuation correction was performed and Figure 8B presents the

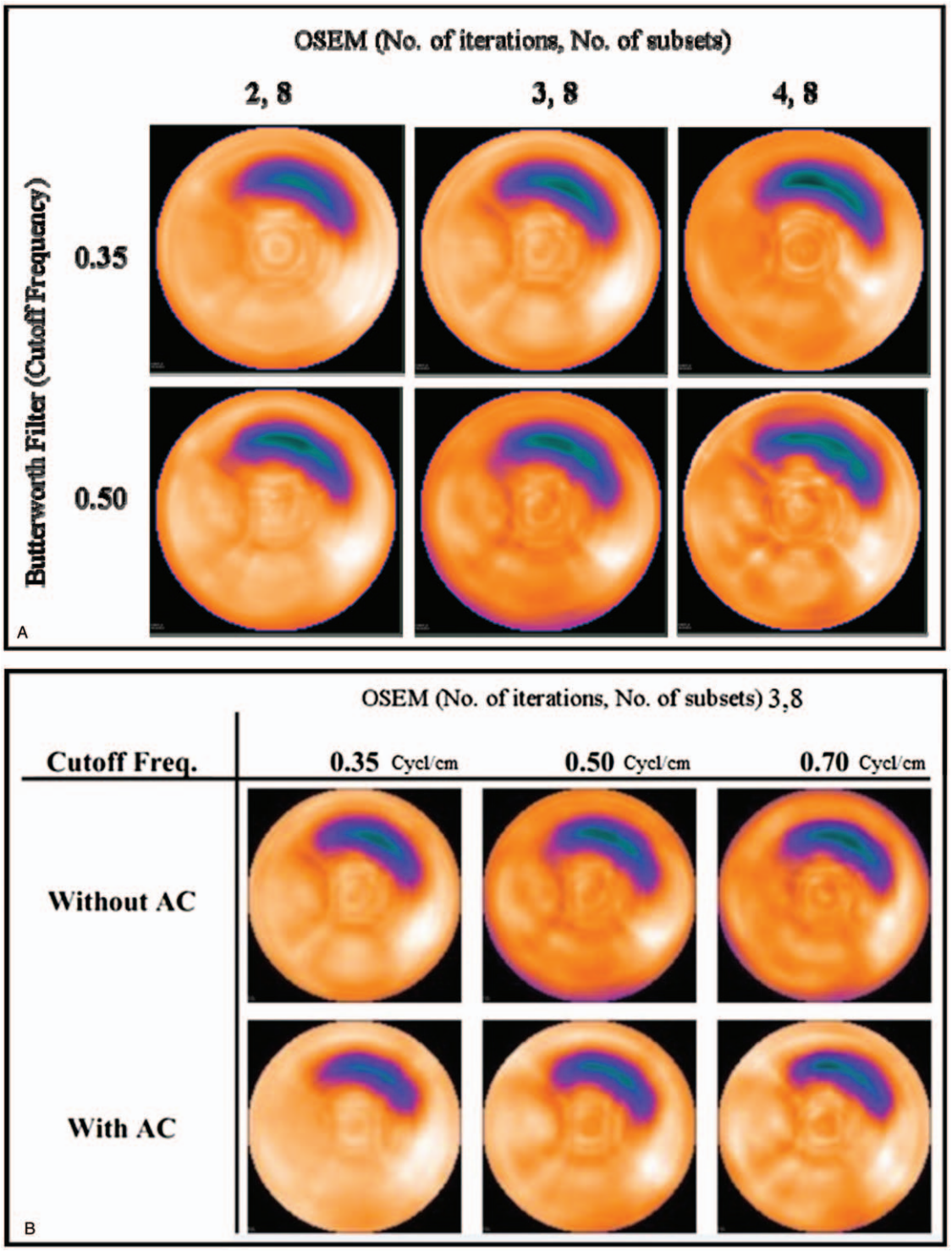

Figure 6. (A) Reconstructed DSPECT polar maps with different number of iterations and subsets in OSEM reconstruction algorithm and different post-filter cut-off frequencies without AC. (B) Reconstructed DSPECT polar maps with the same number of iterations and subsets in OSEM reconstruction algorithm and different post-filter cut-off frequencies with and without AC. (C) Reconstructed DSPECT polar maps with different number of iterations and subsets in OSEM reconstruction algorithm and the same post-filter cut-off frequency with and without AC. AC = attenuation correction, DSPECT = dynamic single photon emission computed tomography, OSEM = ordered subset expectation maximization.

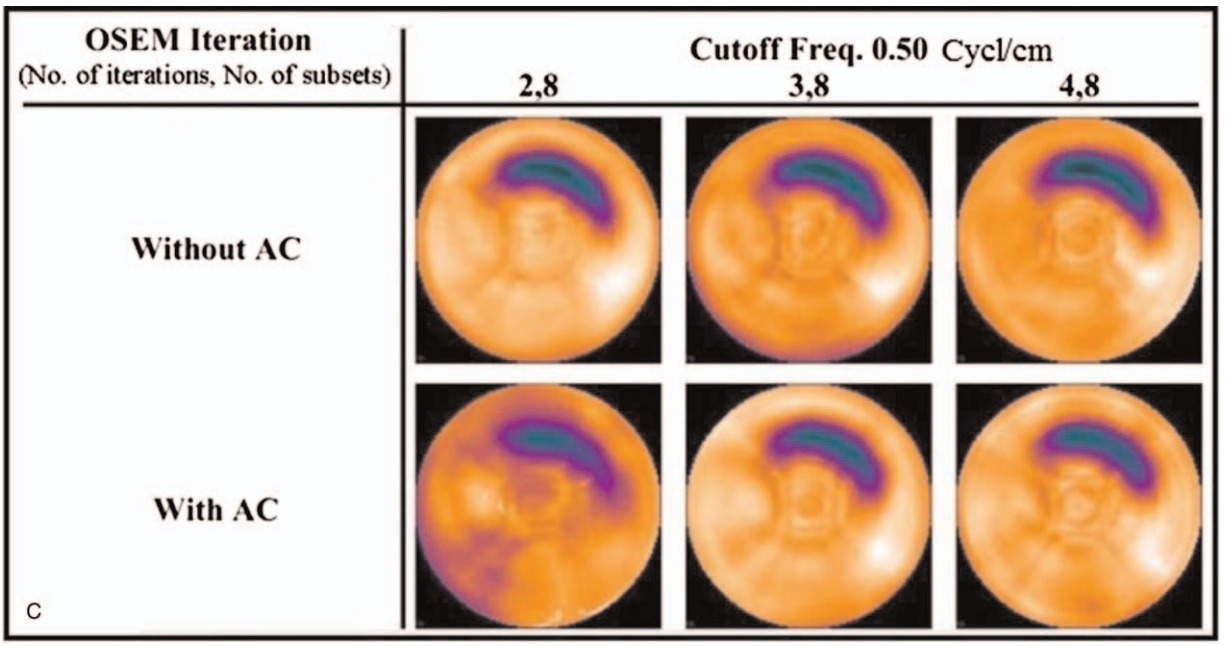

Figure 6. (Continued).

attenuation corrected data values. Figure 8C shows Figure 8A and B in one polar map for better comparison.

4. Discussion

The aim of this study was to evaluate the effect of x-ray-derived attenuation correction along with postprocessing filtering and number of iterations in reconstruction phase in dynamic myocardial perfusion SPECT. To perform that, a modified cardiac torso phantom with a specific defect was used. The radioactivity concentration of both myocardial and defect segment of phantom could be changed from outside the tank. This phantom was used to simulate the dynamic behavior of blood flow in heart. The washout rate was evaluated both in

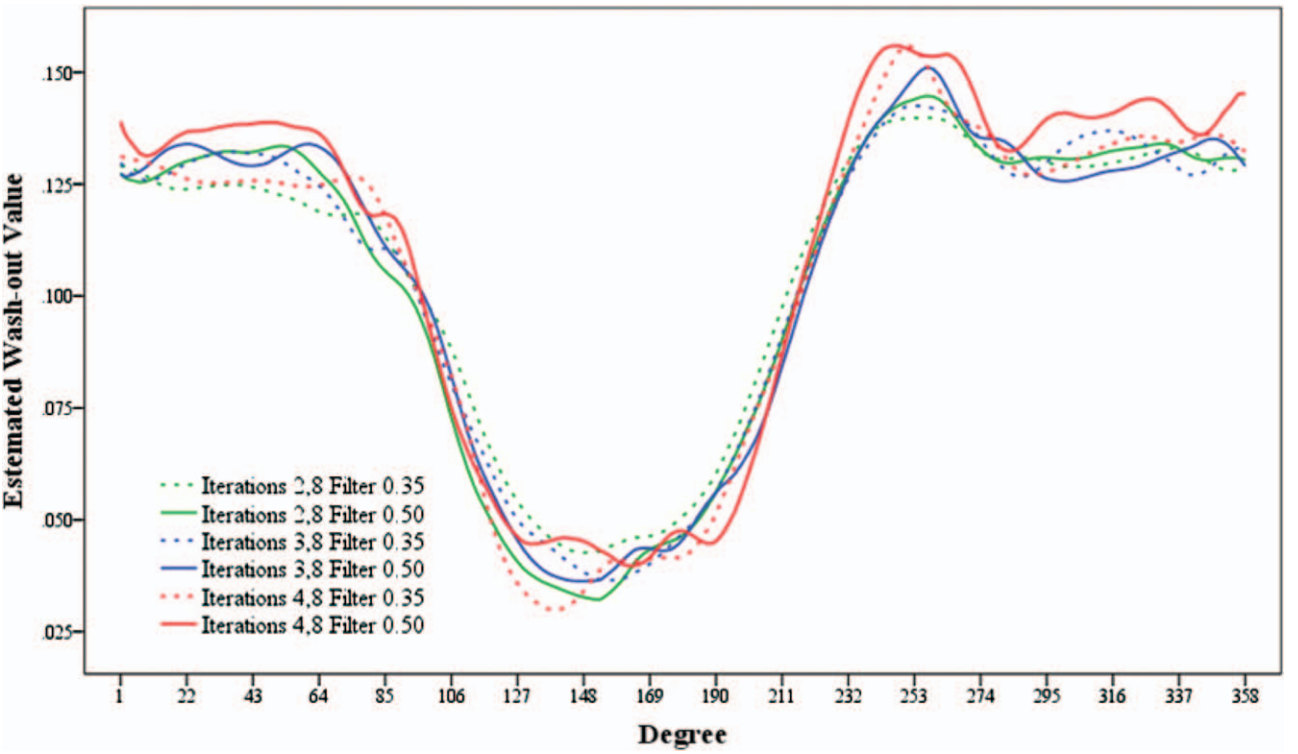

Figure 7. The extracted profiles from a disk-like line in the polar maps view where the middle of the defect region is crossed.

Table 1

Full width at half maximum (FWHM) for different reconstructions.

Iterations	Cut-off frequency, cycle/cm	FWHM*
2, 8	0.35	104.11 ± 1.50
	0.50	110.39 ± 0.54
3, 8	0.35	109.32 ± 2.00
	0.50	114.02 ± 1.24
4, 8	0.35	113.12 ± 0.94
	0.50	118.04 ± 0.76

*Full width at half maximum.

normal and defect area in response with either attenuation correction or reconstruction iterations number or post-filtering.

In the hose coupling point, the radioactivity concentration was somehow out of control. Therefore the mid-inferoseptal portion of the LV wall shows higher washout rate in all reconstructed images. To verify that reported high washout rate originated from the hose coupling, the experiment was repeated with different defects (with variation both in size and position). All the experiments show the same phenomenon in the hose coupling point. In Figure 5, the approximate position of defect is obtained.

As discussed briefly in Section 1, we have to reduce the time per projection in DSPECT to achieve sufficient temporal resolution. By this, the accumulated counts in each projection could be dramatically low which leads to low signal-to-noise ratio

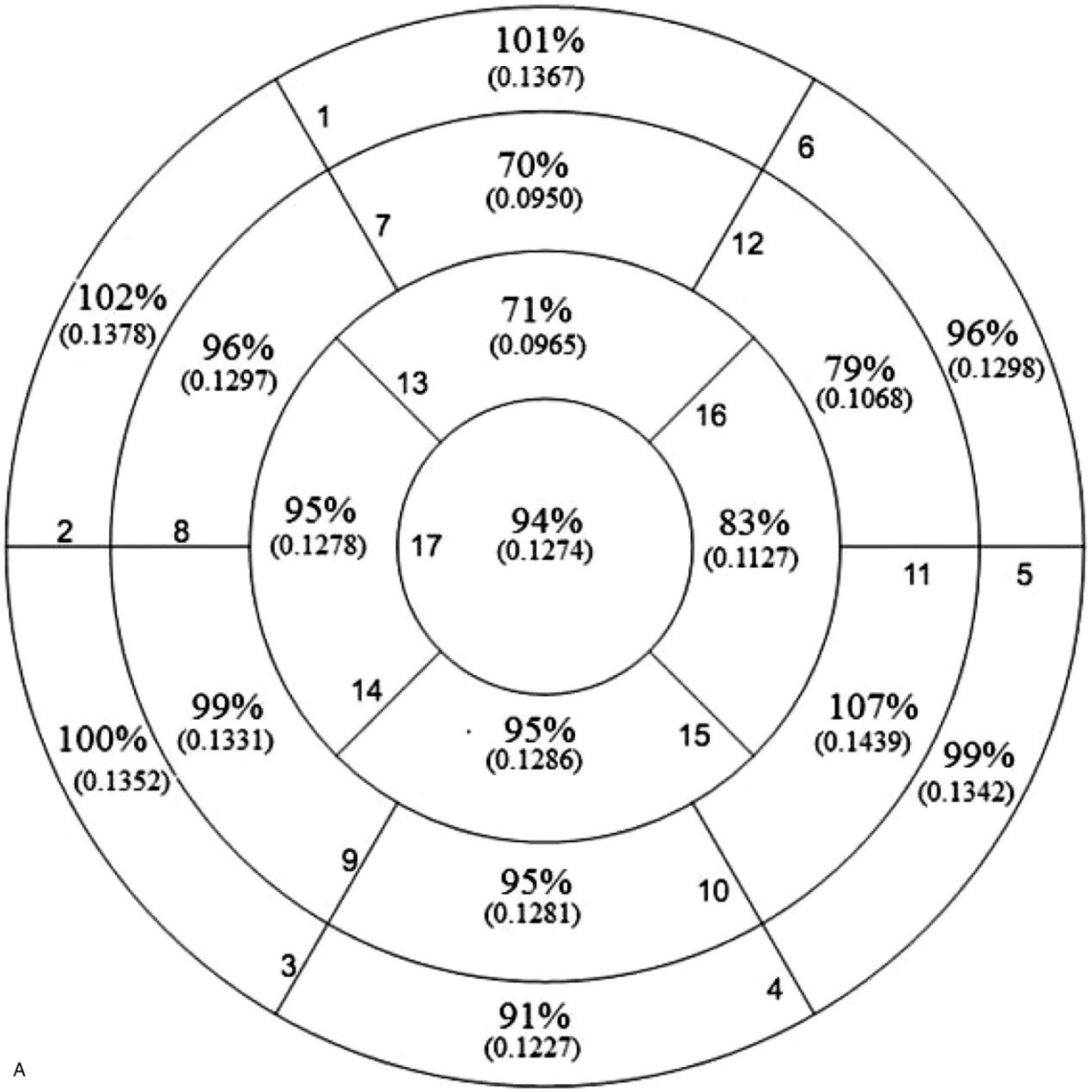

Figure 8. (A) Mean value of washout rate in each segment divided by desired washout rate in normal region (0.135) in percentage. The mean values are depicted in parenthesis. The reconstruction parameters: OSEM 3, 8 BW 0.5—with AC. (B) Mean value of each segment divided by desired washout rate in normal region (0.135) in percentage. The mean values are depicted in parenthesis. The reconstruction parameters: OSEM 3, 8 BW 0.5—without AC. (C) (A) and (B) in one polar map. The underlined numbers are for (A) and the others (not underlined) are for (B). Mean value of each segment divided by desired washout rate in normal region (0.135) in percentage. AC = attenuation correction, OSEM = ordered subset expectation maximization.

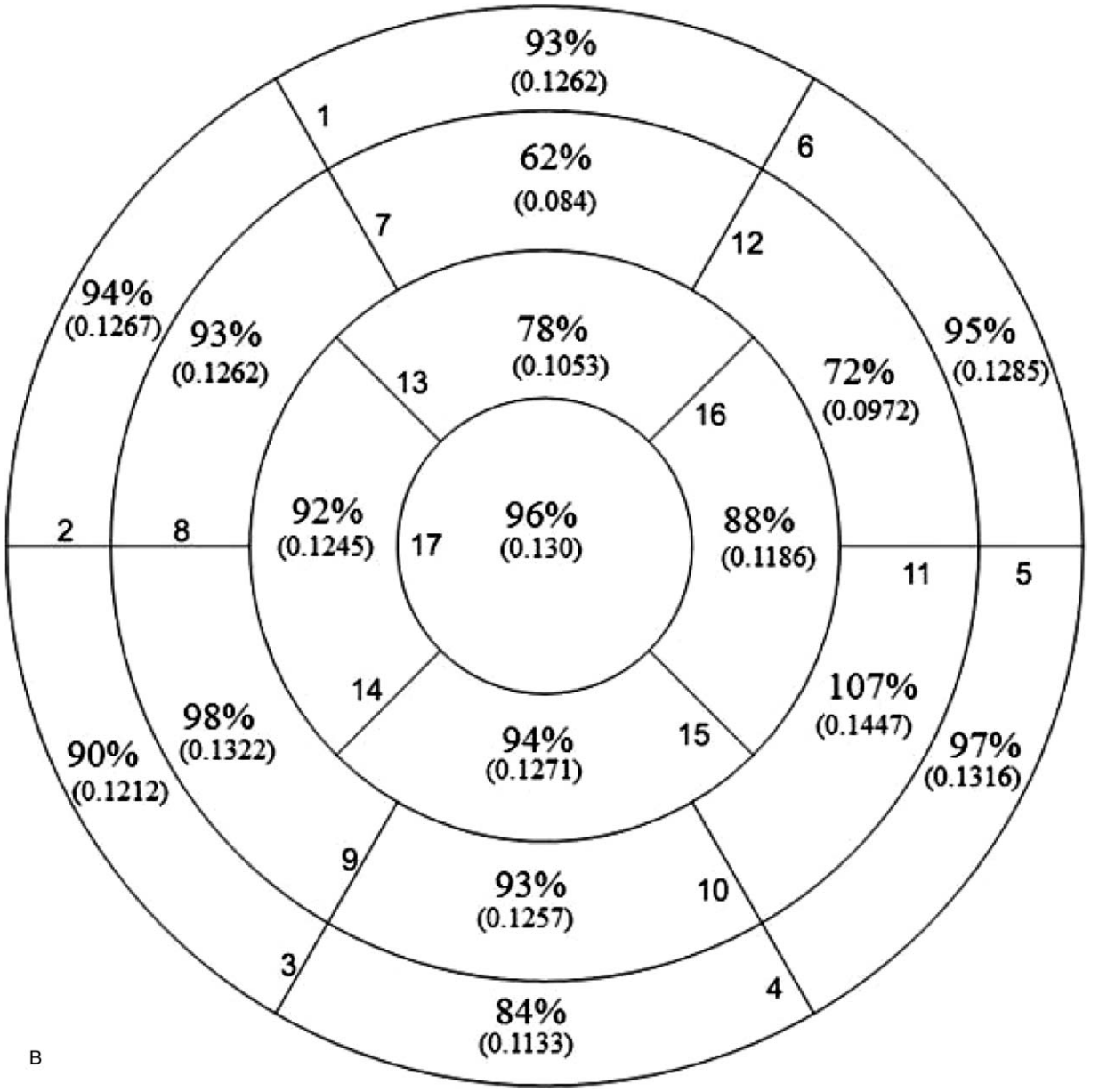

Figure 8. (Continued).

projections.[7] So, every endeavor that causes either noise reduction or signal strengthening can be of interest. Post reconstruction filtering can effectively reduce the noise in final result. However, intense filtering may affect the main signal and impose error to the final interpretation and reduced the details.[25]

As reported by Van Laere et al[30] and Heller and Hendel[31] the proper filter choice depends on:

1. The energy and administered activity.
2. Number of counts.
3. The statistical noise and the background noise level.
4. The organ which is examined.
5. The type of information sought from images (such as quantitative, localization).
6. The collimator type.

Accordingly, as suggested, the proper filter parameters for each SPECT examination should be standardized empirically (filtering in SPECT image reconstruction). Hence, we evaluated the effect of filtering parameters on the washout ratio extracted from conventional DSPECT.

Similarly, the number of iterations in OSEM reconstruction method can affect the final result. Increasing the iterations number, the signal values may be estimated more correctly and spatial resolution is increased but such increment, results in higher degree of noise in final image[32] with the increase in the number of image updates (product of the number of iterations and subsets). Thus, it is important to optimize parameters in order to obtain the best needed information from the images.

The parameters of the iterative methods depend upon each examination and the protocol which performs in the department.[33]

As it was predicted, Figure 6A shows that if either the number of iterations or cut-off frequency increases the defect shape will become inhomogeneous in the final washout polar map.

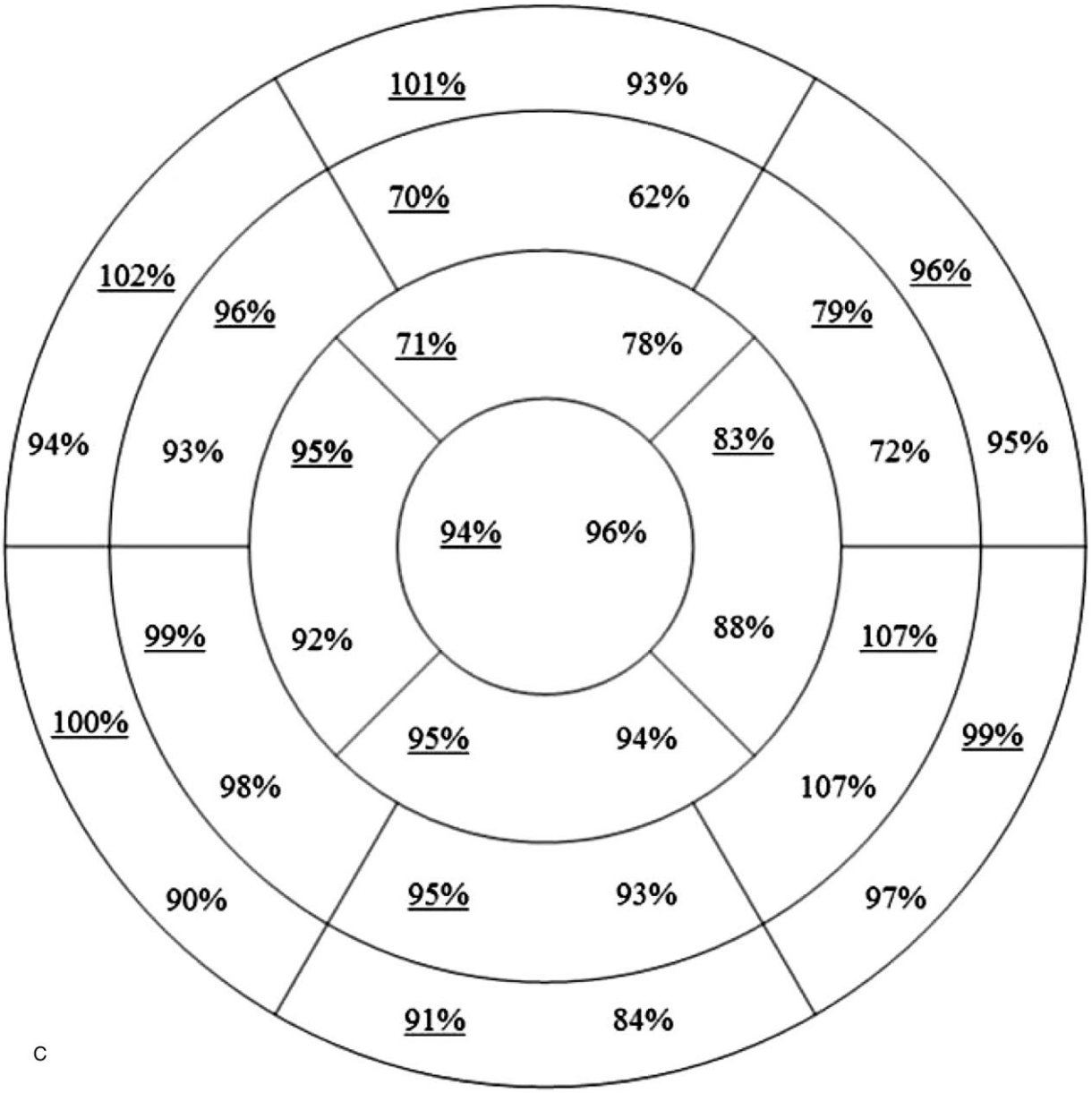

Figure 8. (Continued).

Smoothness of the final washout polar map is obvious in the top left corner map in Figure 6A. Table 1 and Figure 7 show that if a postreconstruction low-pass filter with lower cut-off frequency is applied the extent of estimated effect shortens. Table 1 clearly compares the FWHMs of different curves of Figure 7. This diminution is also meaningful when the number of iterations in reconstruction phase reduces. Since filtering and low number of iterations blurs each reconstruction map, hot areas permeate to the cold areas. It means the calculated defect size will be reduced. As it occurs in the entire time sequence in count maps, the final

Table 2

Mean value $(min)^{-1}$ and standard deviation (%) of the chosen normal and defective region for different reconstructions.

Iterations	Cut-off frequency, cycle/cm	Normal region (mean ± SD)	Defect region (mean ± SD)
2, 8	0.35	0.129 (2.05)	0.061 (26.03)
	0.50	0.130 (2.07)	0.056 (35.49)
3, 8	0.35	0.131 (2.76)	0.059 (31.82)
	0.50	0.129 (3.95)	0.058 (31.34)
4, 8	0.35	0.131 (2.83)	0.053 (33.69)
	0.50	0.138 (3.99)	0.056 (27.80)

washout polar maps may faces a similar occurrence. Moreover, the data in Table 1 tells us that the effect of filtering on FWHM is more powerful than the number of iterations.

Table 2 describes the effect of filtering on the calculated washout value. As it is shown, there is not any remarkable change in the mean value of normal region washout value as the filtering strength rises. But a slight increase is seen in deviation of calculated values within the ROI as the cut-off frequency increases. This growth is more noteworthy when the number of iterations in the reconstruction phase increases. This could be predictable as the filtering smoothes the variation within a uniform area, while it maintain the mean value.

In the defect area, any specific relation between the mean and the minimum and the standard-variation of calculated washout value to either the filtering cut-off frequency or the number of iterations could not be found. On the other hand, the attenuation correction may partly offsetting the gains in bias by reducing the heterogeneity and increase the estimated count values in some regions but the image noise may raises up. Since in conventional reconstruction method in DSPECT a sequence of reconstructed images is used to create time activity curves (TAC) for each voxel and finally the washout rate is extracted from the fitted equation to the TAC, the question arises, "whether or not the final calculated washout would alter if the change in estimated count for each voxel was in similar trend for entire reconstructed images (in each time point)." To find the answer, the effect of attenuation correction is evaluated on the washout values.

The importance of necessary corrections for dynamic cardiac SPECT was reported by Hutton and Ben-Haim[20] although the positive effect of attenuation correction remains unclear in that paper. Previously it was shown that a rational parameter such as myocardial flow reserve could compensate the regional attenuation effects in final results.[34,35]

The myocardial tissue time–activity curve originates from convolution of K1 with the arterial input function.[36] Thus, because the average attenuation for the input function and the myocardium are similar, the average attenuation effects of myocardium segments are largely cancelled out.[37] Nevertheless, AC consistently decreases the SD of the regional TAC, suggesting that AC improves regional myocardial flow estimation.[37]

Since in our conventional reconstruction method the average attenuation effects for each myocardium segments is the same during the whole acquisition time, the calculated count change ratio is predicted to be partly the same in attenuation corrected versus non corrected results.

Phantom is positioned on the table in such a way that the apex region has the least distance to the detector heads, while the septum region faced the most attenuators. Consequently, when the attenuation correction was performed the accumulated counts in the static short axis images corrected upward in the basal and mid-parts of myocardium in each reconstructed image. This increment was more remarkable in septum and inferior parts. (The time sequence reconstructed images are not shown here).

Accordingly, when the washout value was extracted from those images, the attenuation corrected polar map shows increment in the washout values in the basal and mid-parts (regions 1–12). This development in septum and inferior parts is to a greater extent than anterior and lateral parts; whereas a slight reduction is seen in the apical anterior and apical lateral walls. All of these can be observed in Figure 8.

According to these developments, the attenuation corrected normal washout value bias is lower than nonattenuation corrected normal washout value. But the defect severity is underestimated. Although, previously it was shown that the defect severity in the heart wall of the chest phantom did not change significantly as a function of its position in attenuation corrected images versus non-attenuation corrected ones,[38] but our results show that the change in defect severity with attenuation correction depends on its position. Therefore, further surveys are needed to find the relation between the variation of defect severity and its position in the attenuation corrected DSPECT.

5. Conclusion

According to results, the number of iterations in reconstruction phase and postreconstruction filtering affect the washout parameter acquired with cardiac dynamic SPECT protocol. As described in discussion part, the lower cut-off frequency results in the smoother washout value map. Also the defect size would be smaller while using a lower cut-off frequency. The lower number of iterations in OSEM reconstruction algorithm has the same effect on defect. Moreover, we saw that postreconstruction low-pass filter reduces the variance of calculated washout value in normal region while the bias is preserved. To a slightly higher degree, reducing the number of iterations has a similar outcome. But we could not see any similar lineament in the washout value in defect region. Maybe more survey with different degree of filtering on different defects size and different defects severity and position are needed to determine any specific relation. On the other hand, we showed that the attenuation correction may improve the bias of calculated normal washout value. It will amplify the computed washout value in such a voxel that faces a high degree of attenuator toward the detectors. The effect of attenuation correction on the defective washout value could not be answered comprehensively here. We can conclude that if a defect exists in mid-anterolateral portion of myocardium, the computed washout value of that may be slightly underestimated while attenuation correction performed.

Acknowledgment

The authors would like to thank the staff of nuclear medicine department of Namazi Teaching Hospital for their cooperation.

Author contributions

Conceptualization: Mohammadreza Mohseni, Reza Faghihi, Seyed Mohammad Entezarmahdi.
Data curation: Mohammadreza Mohseni, Mahdi Haghighatafshar, Seyed Mohammad Entezarmahdi.
Formal analysis: Mohammadreza Mohseni, Reza Faghihi, Seyed Mohammad Entezarmahdi.
Investigation: Mohammadreza Mohseni, Reza Faghihi.
Methodology: Seyed Mohammad Entezarmahdi.
Resources: Mahdi Haghighatafshar.
Software: Mohammadreza Mohseni, Seyed Mohammad Entezarmahdi.
Supervision: Reza Faghihi, Mahdi Haghighatafshar.
Validation: Seyed Mohammad Entezarmahdi.
Visualization: Mahdi Haghighatafshar, Seyed Mohammad Entezarmahdi.
Writing – original draft: Mohammadreza Mohseni, Reza Faghihi, Mahdi Haghighatafshar, Seyed Mohammad Entezarmahdi.

Writing – review & editing: Mohammadreza Mohseni, Mahdi Haghighatafshar.

References

[1] Haghighatafshar M, Gheisari F, Ghaedian T. Importance of heparin provocation and SPECT/CT in detecting obscure gastrointestinal bleeding on 99mTc-RBC scintigraphy: a case report. Medicine 2015; 94:e1325.

[2] Haghighatafshar M, Farhoudi F. Is brown adipose tissue visualization reliable on 99mTc-methoxyisobutylisonitrile diagnostic SPECT scintigraphy? Medicine 2016;95:e2498.

[3] Fallahi B, Haghighatafshar M, Farhoudi F. Comparative evaluation of the diagnostic accuracy of 99mTc-sestamibi gated SPECT using five different sets of image acquisitions at stress and rest phases for the diagnosis of coronary artery disease. Am J Nucl Med Mol Imaging 2014;4:10–6.

[4] Ficaro EP. Imaging guidelines for nuclear cardiology procedures. J Nucl Cardiol 2006;13:888.

[5] Shahpouri Z, Kamali-Asl A, Bitarafan-Rajabi A, et al. A comparative assessment of dynamic and conventional thallium-201 SPECT myocardial perfusion imaging: Monte Carlo simulations and case studies. Front Biomed Technol 2015;1:91–102.

[6] Kadrmas D, DiBella E, Khare H, et al. Static versus dynamic teboroxime myocardial perfusion SPECT in canines. IEEE Trans Nucl Sci 2000; 47:1112–7.

[7] Slomka P, Berman DS, Germano G. Myocardial Blood Flow from SPECT. J Nucl Cardiol 2017;24:278–81.

[8] Gullberg GT, editor. Dynamic SPECT imaging: Exploring a new frontier in medical imaging. Biomedical Imaging: Nano to Macro, 2004 IEEE International Symposium on; 2004: IEEE.

[9] Reutter BW, Gullberg GT, Huesman RH, editors. Spatiotemporal scatter models for dynamic SPECT. Nuclear Science Symposium Conference Record, 2004 IEEE; 2004: IEEE.

[10] Niu X, Yang Y, Wernick MN, editors. Temporal regularization in fully 5D reconstruction of cardiac gated dynamic SPECT images. Biomedical Imaging: From Nano to Macro, 2011 IEEE International Symposium on; 2011: IEEE.

[11] Links JM, Frank TL, Becker LC. Effect of differential tracer washout during SPECT acquisition, Journal of nuclear medicine: official publication. Soc Nucl Med 1991;32:2253–7.

[12] Zan Y, Boutchko R, Huang Q, et al. Fast direct estimation of the blood input function and myocardial time activity curve from dynamic SPECT projections via reduction in spatial and temporal dimensions. Med Phys 2013;40:092503.

[13] Winant CD, Zelnik YR, Reutter BW, Sitek A, Bacharach SL, Gullberg GT, et al., editors. Analysis of dynamic SPECT/CT measurements of the arterial input function in human subjects. Nuclear Science Symposium Conference Record (NSS/MIC), 2009 IEEE; 2009: IEEE.

[14] Winant CD, Aparici CM, Zelnik YR, et al. Investigation of dynamic SPECT measurements of the arterial input function in human subjects using simulation, phantom and human studies. Phys Med Biol 2011; 57:375.

[15] Reutter BW, Gullberg GT, Huesman RH, editors. Effects of scatter modeling on time-activity curves estimated directly from dynamic SPECT projections. Nuclear Science Symposium Conference Record, 2003 IEEE; 2003: IEEE.

[16] Chiao P-C, Ficaro EP, Dayanikli F, et al. Compartmental analysis of technetium-99m-teboroxime kinetics employing fast dynamic SPECT at rest and stress. J Nucl Med 1994;35:1265–73.

[17] Humphries T. Temporal regularization and artifact correction in single slow-rotation dynamic SPECT. PhD Thesis, Simon Fraser University 2011.

[18] Gullberg GT, Reutter BW, Sitek A, et al. Dynamic single photon emission computed tomography—basic principles and cardiac applications. Phys Med Biol 2010;55:R111.

[19] Koshino K, Fukushima K, Fukumoto M, et al. Breath-hold CT attenuation correction for quantitative cardiac SPECT. EJNMMI Res 2012;2:33.

[20] Hutton BF, Ben-Haim S. What are the Necessary Corrections for Dynamic Cardiac SPECT? 2017;Springer,

[21] Ben-Haim S, Agostini D. Dynamic SPECT: Evolution of a Widely Available Tool for the Assessment of Coronary Flow Reserve. 2015; Springer,

[22] Mohseni S, Kamali-Asl A, Bitarafan-Rajabi A, et al. Effects of filtration on right ventricular function by the gated blood pool SPECT. Ann Nucl Med 2015;29:384–90.

[23] Seret A. The number of subsets required for OSEM reconstruction in nuclear cardiology. Eur J Nucl Med Mol Imaging 2006;33:231.

[24] Brambilla M, Cannillo B, Dominietto M, et al. Characterization of ordered-subsets expectation maximization with 3D post-reconstruction Gauss filtering and comparison with filtered backprojection in 99m Tc SPECT. Ann Nucl Med 2005;19:75–82.

[25] Lyra M, Ploussi A. Filtering in SPECT image reconstruction. J Biomed Imaging 2011;2011:10.

[26] Reutter B, Gullberg G, Huesman R, editors. Direct least squares estimation of spatiotemporal distributions from dynamic cardiac SPECT projections. Nuclear Science Symposium, 1999 Conference Record 1999 IEEE; 1999: IEEE.

[27] Cherry SR, Sorenson JA, Phelps ME. Physics in Nuclear Medicine e-Book. 2012;Elsevier Health Sciences,

[28] Sugai Y, Komatani A, Hosoya T, et al. Comparisons of the time-activity curves of the cardiac blood pool and liver uptake by 99m Tc-GSA dynamic SPECT and measured 99m Tc-GSA blood concentrations. Ann Nucl Med 2006;20:295–301.

[29] Cerqueira MD, Weissman NJ, Dilsizian V, et al. Standardized myocardial segmentation and nomenclature for tomographic imaging of the heart: a statement for healthcare professionals from the Cardiac Imaging Committee of the Council on Clinical Cardiology of the American Heart Association. J Am Soc Echocardiogr 2002;15: 463–7.

[30] Van Laere K, Koole M, Lemahieu I, et al. Image filtering in single-photon emission computed tomography: principles and applications. Comput Med Imaging Graph 2001;25:127–33.

[31] Heller GV, Hendel RC. McGraw-Hill Professional:2017.

[32] Slomka PJ, Patton JA, Berman DS, et al. Advances in technical aspects of myocardial perfusion SPECT imaging. J Nucl Cardiol 2009;16:255–76.

[33] Barros PPd, Metello LF, Camozzato TSC, et al. Optimization of OSEM parameters in myocardial perfusion imaging reconstruction as a function of body mass index: a clinical approach. Radiol Brasil 2015;48:305–13.

[34] Ben-Haim S, Murthy VL, Breault C, et al. Quantification of myocardial perfusion reserve using dynamic SPECT imaging in humans: a feasibility study. J Nucl Med 2013;54:873–9.

[35] Shiraishi S, Sakamoto F, Tsuda N, et al. Prediction of left main or 3-vessel disease using myocardial perfusion reserve on dynamic thallium-201 single-photon emission computed tomography with a semiconductor gamma camera. Circ J 2015;79:623–31.

[36] Efseaff M, Klein R, Ziadi MC, et al. Short-term repeatability of resting myocardial blood flow measurements using rubidium-82 PET imaging. J Nucl Cardiol 2012;19:997–1006.

[37] Wells RG, Marvin B, Poirier M, et al. Optimization of SPECT measurement of myocardial blood flow with corrections for attenuation, motion, and blood-binding compared to PET. J Nucl Med 2017; 117:191049.

[38] Ficaro EP, Fessler JA, Ackermann RJ, et al. Cardiac SPECT: effect of attenuation correction on myocardial tracer distribution. J Nucl Med 1995;36:921–31.